UC Riverside
UC Riverside Previously Published Works

Title

Monitoring Redox Dynamics in Living Cells with a Redox-Sensitive Red Fluorescent Protein

Permalink

https://escholarship.org/uc/item/3jn7125n

Journal

Analytical Chemistry, 87(5)

ISSN

0003-2700

Authors

Fan, Yichong
Chen, Zhijie
Ai, Hui-wang

Publication Date

2015-03-03

DOI

10.1021/ac5041988

Peer reviewed

Development of redox-sensitive red fluorescent proteins for imaging redox dynamics in cellular compartments

Yichong Fan[†], and Hui-wang Ai[†‡]*

[†]Environmental Toxicology Graduate Program, and [‡]Department of Chemistry, University of California Riverside, 501 Big Springs Road, Riverside, CA 92521, United States of America

E-mail: huiwang.ai@ucr.edu

ABSTRACT

We recently reported a redox-sensitive red fluorescent protein, rxRFP1, which is one of the first genetically encoded red-fluorescent probes for general redox states in living cells. As individual cellular compartments have different basal redox potentials, we hereby describe a group of rxRFP1 mutants, showing different midpoint redox potentials for detection of redox dynamics in various subcellular domains, such as mitochondria, the cell nucleus, and endoplasmic reticulum (ER). When these redox probes were expressed and subcellularly localized in human embryonic kidney (HEK) 293T cells, they responded to membrane-permeable oxidants and reductants. In addition, a mitochondrially localized rxRFP1 mutant, Mito-rxRFP1.1, was used to detect mitochondrial oxidative stress induced by doxorubicin□a widely used cancer chemotherapy drug. Our work has expanded the fluorescent protein toolkit with new research tools for studying compartmentalized redox dynamics and oxidative stress under various pathophysiological conditions.

Keywords

INTRODUCTION

The biochemistry and functions of eukaryotic cells are organized within distinct cellular compartments separated by physical barriers, such as lipid-containing membranes [1]. Cellular compartmentation is important for eukaryotic biology, since it provides the basis for spatiotemporal regulation of biomolecules, biomolecular reactions, and signaling. Redox signaling and oxidative stress play critical biological roles [2,3], and it is long accepted that redox regulation exists in the major compartments of mammalian cells, such as mitochondria, the cell nucleus, and the secretory pathway [4]. Each of these compartments shows unique redox characteristics, with mitochondria as the most reducing compartments and the endoplasmic reticulum (ER) as the most oxidizing intracellular environments [4]. Changes in the redox states of individual cellular compartments affect, or even sometimes determine, biological consequences [5].

Genetically encoded fluorescent redox probes, such as redox-sensitive green fluorescent proteins (roGFPs) [6,7] and redox-sensitive yellow fluorescent protein (rxYFP) [8], have been instrumental in understanding redox controls and pathways within cellular compartments. Fusing roGFPs or rxYFP with subcellular localization sequences allows precise targeting of these sensors into various subcellular domains [9-11]. Consequently, the fluorescence of these sensors can be monitored with instruments, such as fluorometers, fluorescence plate readers, or fluorescence microscopy to derive information on redox dynamics of individual cellular organelles. Our laboratory recently reported a redox-sensitive red fluorescent protein, rxRFP1, which comprises of a circularly permuted red fluorescent protein (cpRFP) with cysteine residues appended to the N- and C- termini for the formation of a redox-dependent, reversible disulfide bridge [12]. We have demonstrated that, rxRFP1 can be expressed in living mammalian cells to

monitor redox changes induced by various oxidants and reductants, as well as by a glutathione reductase inhibitor, 2-AAPA [12]. In the basal state, rxRFP1 simultaneously maintained an oxidized and a reduced portion in HEK 293T cells, suggesting that the midpoint redox potential of rxRFP1 is close to the basal redox potential of the cytoplasm. This study has enabled new capabilities for multicolor and multiplex imaging. Moreover, different from roGFPs and rxYFP, which respond to oxidation, either excitation-ratiometrically or inversely, the fluorescence of rxRFP1 is positively related to the extent of oxidation, making rxRFP1 a highly attractive redox sensor [12]. The use of long-wavelength light for excitation of rxRFP1 also reduces the concerns on intracellular oxidation induced by short-wavelength light for excitation of roGFPs [11,13].

Since individual cellular compartments have quite different basal redox states, monitoring redox dynamics in individual compartments therefore requires fluorescent probes with midpoint redox potentials matching the redox state of each compartment. Herein, we report the development of several rxRFP1 mutants (**Figure 1**) showing *in vitro* midpoint redox potentials spanning from − 324 mV to − 244 mV. We also show that the fluorescence of these probes is indicative for redox changes in cellular compartments, including the cell nucleus, mitochondria, and ER. Using a mitochondrially localized rxRFP1.1 mutant, we observed mitochondrial oxidative stress induced by a chemotherapy drug, doxorubicin [14].

MATERIALS AND METHODS

Materials, Reagents, and General Methodology

Synthetic DNA oligonucleotides were purchased from Integrated DNA Technologies (San Diego, CA). Restriction endonucleases were purchased from New England Biolabs (Ipswich, MA) or Thermo Scientific Fermentas (Vilnius, Lithuania). Products of PCR and restriction digestion

were purified by gel electrophoresis and extracted using Syd Laboratories Gel Extraction

columns (Malden, MA). Plasmid DNA was purified using Syd Laboratories Miniprep columns.

All chemicals were purchased from Sigma-Aldrich (St. Louis, MO) or Fisher Scientific

(Hampton, NH) and used as received. DNA sequences were analyzed by Retrogen (San Diego,

CA).

Construction of *Escherichia coli* Expression Plasmids and Libraries

pBAD-rxRFP1 [12] were used as our cloning template. Oligonucleotide pBAD_F (see

Electronic Supplementary Material Table S1) was paired with either RCK_R, or RCE_R, or

RCS_R in individual polymerase chain reactions (PCR) to directly generate rxRFP1 mutants

with point mutations at residue 262. In addition, oligonucleotides 3X_F and 3X_R, which

contain degenerate NNK codons (in which N = A, T, G, or C, and K = G or T), were used to

generate a C262S point mutation and full randomization at residues 1-3 and 263-265. All

amplified DNA fragments were treated with Xho I and Hind III, and ligated into a predigested

compatible pBAD/His B plasmid (Life Technologies, Carlsbad, CA). The resultant ligation

products were used to transform DH10B *Escherichia coli* cells, which were next plated on LB

agar plates supplemented with ampicillin (100μg/mL) and L-arabinose (0.04%, w/v%).

Library Screening

To screen the library generated from oligonucleotides 3X_F and 3X_R, we used a laboratory-

built colony fluorescence imaging system, which has been described previously [12], to evaluate

fluorescence intensities of individual colonies on LB agar plates after overnight incubation at

37°C. We used a digital camera and ImageJ [15] to quantify red fluorescence intensities of

individual colonies. Moreover, a pair of forensic red goggles with a cutoff wavelength at ∼ 590

nm was utilized to assist in identification of bacterial colonies on LB agar plates by human eyes.

Colonies with high to mediocre brightness were selected and cultured in 5 mL liquid LB

supplemented with 100 µg/mL ampicillin and 0.04% L-arabinose. Cells were first incubated at

37°C and 250 rpm overnight, and next, at room temperature and 200 rpm for another 6 h. After

centrifugation to pellet the cells, B-PER Bacterial Protein Extraction Reagents (Pierce, Rockford,

IL) were added, followed by another centrifugation step to remove cell debris. Before and after a

15-min dithiothreitol (DTT, 100 mM) treatment at room temperature, we quantified the

fluorescence of the resultant cell lysates on a monochromator-based Synergy Mx Microplate

Reader (BioTek, Winooski, VT) with excitation and emission wavelengths at 540 nm and 600

nm, respectively. We selected mutants showing large ratios of fluorescence intensities before and

after DTT treatment for further characterization.

Protein Purification and *in vitro* Characterization

His$_6$-tagged proteins were purified using Ni-NTA agarose beads (McLab, South San Francisco,

CA) by following a manufacturer's suggested procedure. Next, they were buffer-exchanged into

Tris-HCl (5mM, pH7.4) using Thermo Scientific Snakeskin dialysis tubing (7k molecular weight

cutoff). Absorption and fluorescence spectra, quantum yields, molar absorption, and pH

sensitivity (pK$_a$) were determined as previously described [12]. To prepared reduced proteins,

protein stocks were incubated in DTT (50 mM) overnight in a nitrogen (N$_2$) glove box. DTT was

removed using Sartorius Vivaspin 500 ultrafiltration columns (Viva Products, Littleton, MA)

right before other characterization experiments. To determine the fluorescence responses of

proteins to mixtures of oxidized and reduced glutathione (GSSG/GSH) showing different redox

potentials, proteins (1 µM) were incubated with GSSG (from 1 to 2000 µM) and GSH (from 1 to

100 mM) overnight in N$_2$-purged Tris-HCl buffer (100mM), and allowed to equilibrate in the N$_2$

glove box at room temperature. Fluorescence intensities were next quantified using a monochromator-based Synergy Mx Microplate Reader. The equilibrium constant for oxidation reactions, K_{ox}, was determined by fitting the data to $F = F_{red} + (F_{ox}-F_{red})/ (1+([GSH]^2/[GSSG])/K_{ox})$, where F_{red} and F_{ox} represent the fluorescence of reduced and oxidized proteins, respectively. The half-reaction of rxRFP reduction is: $rxRFP_{ox} + 2H^+ + 2e^- \rightleftharpoons rxRFP_{red}$, and the half-reaction of GSSG reduction is: $GSSG + 2H^+ + 2e^- \rightleftharpoons GSH$. Based on the standard redox potential of the GSH/GSSG redox pair at pH 7 [16,6], the redox potentials of rxRFPs could then be calculated from the Nernst equation, $E = E^{\varnothing} + \dfrac{RT}{nF} \ln K_{ox}$, where $E^{\varnothing}$ is the standard redox potential of the GSH/GSSG pair, R is the gas constant ($8.315\ J \cdot K^{-1}\ mol^{-1}$), T is the absolute temperature, n is the number of transferred electrons, and F is the Faraday constant (9.649×10^4 $C \cdot mol^{-1}$). To further correct for the pH difference, the redox potential ($E_{7.4}$) at pH 7.4 can be derived from the redox potential (E_7) at pH 7 using the following equation:

$$E_{7.4} = E_7 - \frac{2.303\,RT}{F} \times (7.4 - 7) \quad [6].$$

Construction of Mammalian Expression Plasmids

To create a plasmid for mitochondrial expression of rxRFP1.1, we used oligonucleotides Mito_F and Mito_RCK_R, and Mito_RCK_F and rxRCK_R to amplify a mitochondrial targeting sequence (MLSLRQSIRFFKPATRTLCSSRYLL) from pMito-hsGFP [17] and the rxRFP1.1 gene fragment from pBAD-rxRFP1.1, respectively. Next, an overlap PCR with oligonucleotides Mito_F and rxRCK_R was utilized to assemble the two fragments. The resultant DNA was digested with Hind III and Xba I, and then ligated into a predigested pcDNA3 plasmid to

generate pMito-rxRFP1.1. To construct a plasmid for ER localization of rxRFP1.4, we used oligonucleotides ER_RCS_F1, ER_RCS_F2, ER_RCS_F3, and ER_RCS_R to amplify the rxRFP1.4 gene fragment from pBAD-rxRFP1.4 and further extend it to include an N-terminal ER localization sequence (MLLSVPLLLGLLGLAAAD) and a C-terminal ER retention sequence (KDEL). The resultant DNA was again digested with Hind III and Xba I, and then ligated into a predigested pcDNA3 plasmid to generate pER-rxRFP1.4. To construct a plasmid for nuclear expression of rxRFP1, we used oligonucleotides Nuc_F, RCC_Nuc1, Nuc2, and Nuc3 to amplify the rxRFP1 gene fragment from pBAD-rxRFP1 and further extend it to include C-terminal three repeats of a nuclear localization sequence (DPKKKRKV). The PCR product was digested with Hind III and Xba I and ligated into a predigested pcDNA3 plasmid to derive pNuc-rxRFP1. A pNuc-rxRFP1.1 plasmid was also generated based on the same strategy, except for that the oligonucleotide RCK_Nuc1 was used to replace RCC_Nuc1 to amplify rxRFP1.1 from pBAD-rxRFP1.1 in the initial PCR reaction. To construct a plasmid for cytosolic expression of rxRFP1, we used oligonucleotides NESrxRFP_F1, NESrxRFP_F2, NESrxRFP_F3, and NESrxRFP_R to amplify the rxRFP1 gene fragment from pBAD-rxRFP1 and further extend it to include an N-terminal nucleus export signal (LQLPPLERLTL). The product was digested with Hind III and Xba I, and then ligated into a predigested pcDNA3 plasmid. Another two copies of the nucleus export signal peptide were further appended to the C-terminus of rxRFP1. Two pairs of oligonucleotides, NEScopy2_F and NEScopy2_R, and NEScopy3_F and NEScopy3_R, were separately annealed to form double-stranded DNA fragments, which were next treated with Xba I and EcoR I, and EcoR I and Apa I, respectively. The DNA fragments were inserted between the corresponding restriction sites of the above pcDNA3-derived plasmid to afford pNES-rxRFP1.

Cell Culture, Transfection, and Staining

HEK 293T cells were cultured in Dulbecco's Modified Eagle's Medium (DMEM) supplemented with 10% fetal bovine serum (FBS), and incubated at 37°C under 5% CO_2 in humidified air. The day before transfection, approximately 2.5×10^5 cells were seeded into individual 35-mm culture dishes. In the next day, 3 µg plasmid DNA and 9 µg PEI (polyethylenimine, linear, M.W. 25 kD) were mixed in fresh DMEM (500 µL) with no FBS. After incubation at room temperature for 15 min, the mixture was added into a 35-mm cell culture dish containing HEK 293T cells. Three hours later, the culture medium was replaced with fresh DMEM containing 10% FBS. Cells were cultured for another 48 h. To stain cells, Rhodamine 123 or 4',6-diamidino-2-phenylindole (DAPI) was diluted with Dulbecco's Phosphate Buffered Saline containing 1 mM Ca^{2+} and 1 mM Mg^{2+} (DPBS++) to a final concentration of 1 µg/mL. Cells were next incubated in the staining solution for 15 min at room temperature, followed by two times of wash with 2 mL DPBS++ over 15 min.

Fluorescence Imaging

Cells were washed twice with 2 mL DPBS++, and left in 1 mL DPBS++ for immediate imaging on a Motic AE31 inverted epi-fluorescence microscope with a 20× objective lens or a Leica SP5 confocal fluorescence microscope with a 40× objective lens. The Motic AE31 microscope was equipped with a 100-W Short-Arc Mercury lamp, a 540/25 nm excitation filter, a 565 nm longpass dichroic mirror, and a 605/55 nm emission filter for imaging rxRFPs. The Leica SP5

microscope was equipped with a 405 nm diode laser to excite blue fluorescent dyes, an argon-ion

laser with 488 nm to excite green fluorescent probes, and a HeNe laser with 543 nm to excite

rxRFPs. The Leica SP5 was also equipped with a highly sensitive prism spectral detector, and

420 - 480 nm, 495 - 550 nm, and 560 - 650 nm were utilized to collect fluorescence emission for

blue, green, and red fluorescent probes, respectively. For time-lapse series, images were acquired

every min and stimulating chemicals were added between acquisitions. To study redox responses

of rxRFP mutants in various cellular compartments, we sequentially treated cells with Aldrithiol-

2 (AT-2, 1 mM) and DTT (10 mM). To establish a fully reduced state for rxRFP1.4 in the ER, we

permeabilized cells with 0.02% (w/v) digitonin for 10 min before addition of DTT. The intensity

values before treatment (F_0) and in the fully oxidized (F_{ox}) and reduced (F_{red}) states were utilized

to estimate the percentages of oxidized rxRFP proteins based on the equation: $\dfrac{F_0 - F_{red}}{F_{ox} - F_{red}} \times 100$.

The basal redox potentials were next calculated based on the Nernst equation. To correct for the

pH difference, the redox potential (E') at any pH can be derived from the redox potential ($E_{7.4}$) at

pH 7.4 using the following equation: $E_{pH} = E_{7.4} - \dfrac{2.303\,RT}{F} \times (pH - 7.4)$ [6].

To study doxorubicin-induced oxidative stress in cellular compartments, doxorubicin (2 μM)

were added into the cell culture medium at 36 hs after HEK 293T cells were transfected with

corresponding plasmids. Incubation continued at 37°C for another 12 hs. Cells were washed

three times with DPBS++ (2 mL each) right before fluorescence images were taken. To

investigate the concentration-dependency, cells transfected with pMito-rxRFP1.1 were treated

with doxorubicin (from 100 nM to 2 μM), and all other conditions were kept the same. To further

study mitochondrial oxidative stress over time, doxorubicin (2 μM) was used to treat cells and

fluorescence images were taken at intervals over 12 hs. ImageJ [15] was used to process all images. To compare fluorescence intensities of cells under various conditions, integrated intensities from at least three images of replicate samples were used to derive means and standard deviations.

RESULTS AND DISCUSSION

Engineering of rxRFP1 Mutants

We hypothesized that the residues in close proximity to the two cysteine residues (C241 and C261) responsible for the formation of a reversible disulfide bridge between the N- and C-termini of rxRFP1 (**Figure 1**) should be important for the midpoint redox potential of rxRFP1. To test this notion, we introduced point mutations (C262K, C262S, or C262E) to rxRFP1, because C262 is close to C261 but not involved in the formation of the reversible disulfide bridge [12]. We intentionally chose lysine, serine, and glutamate for the replacement, because they represent a positively charged residue, a neutral residue structurally similar to cysteine, and a negatively charged residue, respectively. We further named these three mutants as rxRFP1.1, rxRFP1.2 and rxRFP1.3, respectively (**Figure 1**).

During the evolution of rxRFP1, we previously derived an intermediate mutant, A4-CS [12]. We utilized oligonucleotides containing degenerate codons to create a gene library, for which residues 1-3 and 263-265 (numbered according to rxRFP1) were fully randomized and other parts were identical to A4-CS. The oligonucleotides were also designed to generate products matching the length of rxRFP1. We screened ∼ 10,000 individual colonies on LB agar plates and ∼ 400 clones as cell lysates, based on their fluorescence brightness and responsiveness to DTT reduction. We identified a promising clone, which showed bright red fluorescence and high

responsiveness to DTT. This mutant, which was named rxRFP1.4 (**Figure 1**), is different from

rxRFP1 in seven mutations (E1S/L2P/S3R/C262S/S263R/V264K/A265L).

Midpoint Redox Potentials of rxRFP1 Mutants

The fluorescence of all abovementioned four rxRFP1 variants increased, as the proteins were

converted from their reduced states to oxidized states. Their emission intensities in fully oxidized

states were roughly 4-fold higher than the intensities in fully reduced states (**Table 1**). Moreover,

their fluorescence excitation and emission profiles were also identical to those of rxRFP1.

Exciting each protein at 576 nm generated strong red fluorescence with a peak at 600 nm.

Compared to rxRFP1, the brightnesses of rxRFP1.2 and rxRFP1.3 were reduced, while rxRFP1.1

and rxRFP1.4 were at least 45% brighter than rxRFP1, under either fully oxidized or reduced

conditions (**Table 1**).

We next determined the thermodynamic stabilities of disulfide bonds in these rxRFP1 mutants

(**Figure 2**). We incubated purified proteins with mixtures of reduced and oxidized glutathione

(GSH/GSSG) at pH 7.4. After equilibration at room temperature, their fluorescence intensities

were measured to derive the apparent equilibrium constants for their oxidation reactions (K_{ox} =

83.6 M, 1.71 M, 0.36 M, and 0.22 M for rxRFP1.1, rxRFP1.2, rxRFP1.3, and rxRFP1.4,

respectively), based on the assumption that mixed disulfides between proteins and glutathione

were negligible at equilibrium. Since the standard redox potential of the GSH/GSSG redox pair

is − 240 mV at pH 7 [16], we consequently derived the midpoint redox potentials for rxRFP1.1,

rxRFP1.2, rxRFP1.3, and rxRFP1.4 to be − 324 mV, − 272 mV, − 251 mV, and − 244 mV at pH

7.4, respectively. In parallel, the midpoint redox potential of rxRFP1 was determined to be – 281 mV.

These rxRFP1 mutants have quite different midpoint redox potentials. Placing a positively charged lysine and a negatively charged glutamate at residue 262 increased and reduced the thermodynamic stability of the disulfide bond, respectively. A single-residue difference between rxRFP1.1 and rxRFP1.3 was able to vary the midpoint redox potentials by 73 mV. This trend, however, contradicts our initial assumption and previous knowledge of roGFP and rxYFP mutants that positively charged residues should stabilize thiolate species to weaken disulfide bonds [7]. On the other hand, rxRFP1.4, which was engineered from a randomized library, was enriched with positively charged residues at residues 3, 263, and 264. These mutations indeed reduced the thermodynamic stability of the disulfide bond, leading to the least negative midpoint redox potential among the whole rxRFP family (**Table 1**). Therefore, the interplay between the thermodynamic stability of a disulfide bridge and its surrounding amino acid residues seemed to be rather complex, and cannot be predicted by simply considering side-chain charges. Presumably, other factors, such as steric constraint, shape, and size, may also play important roles.

Imaging of Redox Dynamics in Subcellular Compartments

When the midpoint redox potential of a fluorescent probe matches the basal redox level of a cellular compartment, the probe is maintained as a mixture of reduced and oxidized proteins to detect redox changes toward either directions. Moreover, a small redox-potential shift in this range can cause a relatively large change in fluorescence intensity. Mitochondria are usually considered as the most reducing intracellular organelles, due to a high rate of electron transfer to

molecular oxygen (O_2) during mitochondrial respiration [4]. Therefore, we genetically fused

rxRFP1.1, which has the lowest midpoint redox potential among the whole rxRFP family, with a

mitochondrial targeting sequence (MTS) derived from cytochrome c oxidase subunit IV (COX4).

This fusion construct was expected to result in the expression and localization of rxRFP1.1 in the

mitochondrial matrix. Indeed, HEK 293T cells expressing this construct displayed a clear pattern

of mitochondrial fluorescence (**Figure 3A**), which matches well with the fluorescence pattern of

rhodamine 123, a widely used synthetic probe for mitochondrial membrane potential. Next, we

treated the cells with a cell-permeable oxidant, AT-2 (1 mM), and mitochondrial fluorescence

increased drastically within 3 min (**Figure 3B**). Further addition of a reductant, DTT (10 mM),

evoked an immediate decrease in mitochondrial fluorescence to a level lower than that of the

initial untreated basal state. rxRFP1.1 was fully oxidized or reduced in these cells after addition

of AT-2 or DTT, because supplementing additional AT-2 or DTT did not trigger any further

fluorescence change in either conditions. Based on these intensity values, we estimated that, in

the basal state, ~ 36% of rxRFP1.1 was oxidized in the mitochondrial matrix of HEK 293T cells.

Providing that rxRFP1.1 equilibrates with GSSG and GSH *in vivo* the same as it does *in vitro*, we

further estimated the redox potential for the mitochondrial matrix of HEK 293T cells to be – 329

mV at pH 7.4 and 37°C. Because the pH of mitochondria has been estimated to be 7.98 [18], the

redox potential was further corrected to be – 365 mV at pH 7.98 and 37 °C (**Table 2**), based on

the assumption that the equilibrium between rxRFP1.1 and glutathiones was not affected by pH

changes from 7.4 to 7.98. Our estimated value (– 365 mV) is close to the value (– 360 mV)

reported by Hanson and coworkers [6], who used roGFP1 to estimate the mitochondrial redox

potential of HeLa cells. Our experiments support that rxRFP1.1 is an effective probe for

monitoring both oxidative and reductive changes in mammalian mitochondria.

Since the ER is the most oxidizing intracellular compartment [4], we fused rxRFP1.4, a mutant with the highest midpoint redox potential, with peptide sequences responsible for protein localization and retention in the ER. rxRFP1.4 localized in the ER, as confirmed by co-localization studies with a previously established green fluorescent ER-mWasabi probe [19], responded to treatments of AT-2 (1 mM) and DTT (10 mM), demonstrating its usefulness as a fluorescent probe for redox dynamics in the ER (**Figure 4A & 4B**). We observed that the direct addition of DTT (10 mM) in the imaging medium was unable to fully reduce rxRFP1.4 in the ER, so we further developed a procedure to permeabilize cell membranes with digitonin. We co-treated HEK 293T cells with digitonin (0.02%, w/v) and AT-2 (1 mM) or DTT (10 mM), and estimated that ~ 73% rxRFP1.4 was in the oxidized state before any treatment. We further estimated that the basal redox potential for the ER of HEK 293T cells was − 209 mV at pH 7.0 and 37°C (**Table 2**). This was based on the same assumptions mentioned previously for estimating the redox potential of mitochondria, except for that pH 7.0 was used as the typical pH of the ER [20]. We want to note that the reported values for the redox potential of ER have been quite inconsistent, at least ranging from − 118 mV to − 242 mV [21-24]. The inconsistency in the literature may be caused by several reasons: first, those studies used different organisms or cell lines, and their biological differences may be truly significant; second, cell culture methods and sample preparation may have an impact on the redox states of ER; third, redox sensors and ER-endogenous redox components may not reach a complete thermodynamic equilibrium, and their redox states are kinetically separated, thereby leading to different numbers reflecting the reducing power of different ER redox components [25]. Our derived value is close to the number (− 208 mV at pH 7.0) reported in a recent study [26], which used a glutaredoxin-coupled roGFP to estimate the ER glutathione redox potential in HeLa cells.

To generate fluorescent probes for redox imaging in the cell nucleus, we appended a nuclear localization sequence (NLS) to the C-terminus of either rxRFP1 or rxRFP1.1. Both constructs resulted in proper nuclear localization patterns (**Figure 5A**), as confirmed by co-localization studies with a popular nuclear and chromosome stain, DAPI. However, nuclear rxRFP1 was almost fully reduced, because addition of DTT (10 mM) in the imaging medium did not decrease the fluorescence of rxRFP1. In stark contrast, nuclear rxRFP1.1 could be oxidized by AT-2 (1 mM), and further reduced by DTT (10 mM) to an intensity level lower than the initial state (**Figure 5B**). These data indicate that rxRFP1.1 is better suited for monitoring nuclear redox dynamics than rxRFP1. Different from the oxidation of rxRFP1.1 or rxRFP1.4 in the mitochondria or ER, the oxidation of nuclear rxRFP1.1 by AT-2 (1 mM) quickly induced cellular antioxidant pathways, as oxidized nuclear rxRFP1.1 were reduced spontaneously in a few minutes (**Figure 5B**). The cell nucleus seemed to have a high ability to mitigate oxidative stress to maintain the integrity of the genome, although the exact molecular mechanism requires further investigation. We estimated that ~ 39% of nuclear rxRFP1.1 were oxidized in the untreated basal condition, so the nuclear redox potential of HEK 293T cells was approximately − 326 mV at pH 7.4 and 37°C (**Table 2**).

We further sought to estimate the cytoplasmic redox potential of HEK 293T using rxRFP1. Considering its comparable size to other single fluorescent proteins, the untagged rxRFP1 can likely passively diffuse through the nuclear pore [27]. The observed whole-cell fluorescence was therefore affected by the redox potentials of the cytosol and the nucleus, the redox reaction kinetics of rxRFP1, and the intercompartmental protein-transport kinetics. Indeed, when an rxRFP1-expressing cell was imaged at a high resolution and magnification, the fluorescence of the nucleus seemed to be dimmer than the fluorescence of the cytosol (**Figure 6A**), supporting

that the cell nucleus is more reduced than the cytosol and the cytosol-nucleus rxRFP1-transport is not much faster than the redox reaction of rxRFP1. We next expressed rxRFP1 fused with three copies of a nuclear export signal peptide. The fusion protein was exclusively in the cytosol (**Figure 6B**). We performed the oxidation and reduction experiments with AT-2 (1 mM) and DTT (10 mM), respectively (**Figure 6C**). We estimated that ~ 56% of rxRFP1 was oxidized before treatment, corresponding to a redox potential of − 277 mV for the cytosol of HEK 293T (**Table 2**).

We want to note that the dynamic ranges of these rxRFP probes in cell compartments may not exactly match the dynamic ranges determined *in vitro* with purified proteins, because the absolute fluorescence intensities are often sensitive to other environmental factors (*e.g.* pH, temperature, and ionic strength). However, the redox equilibrium itself is less affected by small environmental changes [8], and it is reasonable to estimate the fractions of oxidized proteins based on the fluorescence intensity values before treatment and in the corresponding fully oxidized and reduced conditions. In fact, in order to estimate the redox potentials for mitochondria (pH 7.98) and the ER (pH 7.0), we assumed that the equilibria between rxRFPs and glutathiones were not changed even though the *in vitro* glutathione titration experiment was done at pH 7.4. We further validated this assumption by incubating rxRFP1.1 or rxRFP1.4 with mixtures of GSH and GSSG at pH 8 and pH 7, respectively. The equilibrium between rxRFP1.1 or rxRFP1.4 and glutathiones at pH 8 or pH 7 was identical to the corresponding equilibrium at pH 7.4 (**Figure 7**), further suggesting that our estimation was appropriate.

Mitochondrial Oxidative Stress Induced by Doxorubicin

Doxorubicin is a chemotherapy drug used to treat a large spectrum of cancer [14]. It interacts with DNA and DNA topoisomerases to inhibit DNA replication and transcription [14]. Doxorubicin is also known to induce oxidative stress, which has been utilized to explain the adverse cardiotoxic effect of chemotherapy [28]. Mitochondria are a major intracellular organelle responsible for the production of reactive oxygen and nitrogen species (ROS/RNS) [29]. To find direct evidences for doxorubicin-induced mitochondrial oxidative stress, we applied doxorubicin (2 μM) to HEK 293T cells, which expressed mitochondrial rxRFP1.1, nuclear rxRFP1.1, or untagged rxRFP1, respectively. Fluorescence intensities increased in all groups, indicating that the cells have shifted to a more oxidized state by doxorubicin (**Figure 8A**). The most prominent fluorescence enhancement (3.68 ± 0.79 fold) was observed for cells expressing mitochondrial rxRFP1.1, suggesting that mitochondrial oxidative stress was severe under this condition. We further treated HEK 293T cells expressing mitochondrial rxRFP1.1 with various concentrations of doxorubicin (200 nM - 2 μM). The fluorescence intensity increased in a dose-dependent manner (**Figure 8B**), and 2 μM DOX induced a maximal response of 3.89 ± 0.55 fold. These aforementioned results were derived from end-point measurements at 12 hs after treatment. We next monitored mitochondrial oxidative stress over time. We stimulated cells with doxorubicin (2 μM), and quantified mitochondrial fluorescence at intervals over 12 hs. The fluorescence started to increase in the first hour, and reached a plateau in about 6 hs, (**Figure 8C**). The results support that doxorubicin indeed causes serious mitochondrial oxidative stress, and our new probes are effective for sensing compartmentalized redox dynamics and oxidative stress in living mammalian cells. Doxorubicin is often administered at 20-50 mg/m^2 every 3 or 4 weeks to treat cancer [30]. In a pharmacokinetics study on patients with AIDS-related Kaposi's Sarcoma, a single dose of 20 mg/m^2 doxorubicin infused over 30 min generated a peak plasma doxorubicin

concentration of 8.34 µg/ml (~ 15 µM) [31]. This further suggests that our observed mitochondrial oxidative stress is likely clinically relevant.

CONCLUSIONS

We have developed several rxRFP mutants showing midpoint redox potentials spanning from −324 mV to − 244 mV, by substituting amino acid residues close to the key cysteine residues of rxRFP1. We targeted these mutants to cellular compartments with basal redox states matching their midpoint redox potentials, and used them to detect redox dynamics in these cellular compartments, including mitochondria, the cell nucleus, and ER. We confirmed that these probes could respond to exogenous addition of oxidants and reductants, and based on these data, we semi-quantitatively estimated the basal redox potentials of several subcellular organelles. When we utilized the probes to detect oxidative stress induced by doxorubicin at clinically relevant concentrations, we observed dose- and time-dependent fluorescence enhancement. These new rxRFP1 mutants have extended our capabilities for studying redox dynamics and oxidative stress at subcellular locations in living cells.

ELECTRONIC SUPPLEMENTARY MATERIAL

Sequences of oligonucleotides used in this work. This material is available via the Internet at http://xxx.xxx (Publishing Editor: please add the exact link).

NOTE

Invited Article for a Special Issue Featuring Young Investigators in ABC

REFERENCES

1. Diekmann Y, Pereira-Leal JB (2013) Evolution of intracellular compartmentalization. Biochem J 449 (2):319-331

2. Gius D, Spitz DR (2006) Redox signaling in cancer biology. Antioxid Redox Signal 8 (7-8):1249-1252

3. Stone JR, Yang S (2006) Hydrogen peroxide: a signaling messenger. Antioxid Redox Signal 8 (3-4):243-270

4. Go YM, Jones DP (2008) Redox compartmentalization in eukaryotic cells. Biochim Biophys Acta 1780 (11):1273-1290

5. Jones DP, Go YM (2010) Redox compartmentalization and cellular stress. Diabetes Obes Metab 12 Suppl 2:116-125

6. Hanson GT, Aggeler R, Oglesbee D, Cannon M, Capaldi RA, Tsien RY, Remington SJ (2004) Investigating mitochondrial redox potential with redox-sensitive green fluorescent protein indicators. J Biol Chem 279 (13):13044-13053

7. Cannon MB, Remington SJ (2006) Re-engineering redox-sensitive green fluorescent protein for improved response rate. Protein Sci 15 (1):45-57

8. Ostergaard H, Tachibana C, Winther JR (2004) Monitoring disulfide bond formation in the eukaryotic cytosol. J Cell Biol 166 (3):337-345

9. Meyer AJ, Dick TP (2010) Fluorescent protein-based redox probes. Antioxid Redox Signal 13 (5):621-650

10. Ren W, Ai HW (2013) Genetically encoded fluorescent redox probes. Sensors 13 (11):15422-15433

11. van Lith M, Tiwari S, Pediani J, Milligan G, Bulleid NJ (2011) Real-time monitoring of redox changes in the mammalian endoplasmic reticulum. J Cell Sci 124 (Pt 14):2349-2356

12. Fan Y, Chen Z, Ai HW (2015) Monitoring redox dynamics in living cells with a redox-sensitive red fluorescent protein. Anal Chem 87:2802-2810

13. Kolossov VL, Beaudoin JN, Hanafin WP, DiLiberto SJ, Kenis PJ, Gaskins HR (2013) Transient light-induced intracellular oxidation revealed by redox biosensor. Biochem Biophys Res Commun 439 (4):517-521

14. Thorn CF, Oshiro C, Marsh S, Hernandez-Boussard T, McLeod H, Klein TE, Altman RB (2011) Doxorubicin pathways: pharmacodynamics and adverse effects. Pharmacogenet Genomics 21 (7):440-446

15. Schneider CA, Rasband WS, Eliceiri KW (2012) NIH Image to ImageJ: 25 years of image analysis. Nat Methods 9 (7):671-675

16. Appenzeller-Herzog C (2011) Glutathione- and non-glutathione-based oxidant control in the endoplasmic reticulum. J Cell Sci 124 (Pt 6):847-855

17. Chen ZJ, Ai HW (2014) A Highly Responsive and Selective Fluorescent Probe for Imaging Physiological Hydrogen Sulfide. Biochemistry 53 (37):5966-5974

18. Llopis J, McCaffery JM, Miyawaki A, Farquhar MG, Tsien RY (1998) Measurement of cytosolic, mitochondrial, and Golgi pH in single living cells with green fluorescent proteins. Proc Natl Acad Sci U S A 95 (12):6803-6808

19. Ai HW, Olenych SG, Wong P, Davidson MW, Campbell RE (2008) Hue-shifted monomeric variants of Clavularia cyan fluorescent protein: identification of the molecular determinants of color and applications in fluorescence imaging. BMC Biol 6:13

20. Kim JH, Johannes L, Goud B, Antony C, Lingwood CA, Daneman R, Grinstein S (1998) Noninvasive measurement of the pH of the endoplasmic reticulum at rest and during calcium release. Proc Natl Acad Sci U S A 95 (6):2997-3002

21. Sarkar DD, Edwards SK, Mauser JA, Suarez AM, Serowoky MA, Hudok NL, Hudok PL, Nunez M, Weber CS, Lynch RM, Miyashita O, Tsao TS (2013) Increased redox-sensitive green fluorescent protein reduction potential in the endoplasmic reticulum following glutathione-mediated dimerization. Biochemistry 52 (19):3332-3345

22. Delic M, Rebnegger C, Wanka F, Puxbaum V, Haberhauer-Troyer C, Hann S, Kollensperger G, Mattanovich D, Gasser B (2012) Oxidative protein folding and unfolded protein response elicit differing redox regulation in endoplasmic reticulum and cytosol of yeast. Free Radic Biol Med 52 (9):2000-2012

23. Kolossov VL, Leslie MT, Chatterjee A, Sheehan BM, Kenis PJ, Gaskins HR (2012) Forster resonance energy transfer-based sensor targeting endoplasmic reticulum reveals highly oxidative environment. Exp Biol Med (Maywood) 237 (6):652-662

24. Lohman JR, Remington SJ (2008) Development of a family of redox-sensitive green fluorescent protein indicators for use in relatively oxidizing subcellular environments. Biochemistry 47 (33):8678-8688

25. Appenzeller-Herzog C (2012) Updates on "endoplasmic reticulum redox". Antioxid Redox Signal 16 (8):760-762

26. Birk J, Meyer M, Aller I, Hansen HG, Odermatt A, Dick TP, Meyer AJ, Appenzeller-Herzog C (2013) Endoplasmic reticulum: reduced and oxidized glutathione revisited. J Cell Sci 126 (Pt 7):1604-1617

27. Miyawaki A (2011) Proteins on the move: insights gained from fluorescent protein technologies. Nat Rev Mol Cell Biol 12 (10):656-668

28. Chatterjee K, Zhang J, Honbo N, Karliner JS (2010) Doxorubicin cardiomyopathy. Cardiology 115 (2):155-162

29. Stowe DF, Camara AK (2009) Mitochondrial reactive oxygen species production in excitable cells: modulators of mitochondrial and cell function. Antioxid Redox Signal 11 (6):1373-1414

30. Zhang S, Liu X, Bawa-Khalfe T, Lu LS, Lyu YL, Liu LF, Yeh ET (2012) Identification of the molecular basis of doxorubicin-induced cardiotoxicity. Nat Med 18 (11):1639-1642

31. Duggan ST, Keating GM (2011) Pegylated liposomal doxorubicin: a review of its use in metastatic breast cancer, ovarian cancer, multiple myeloma and AIDS-related Kaposi's sarcoma. Drugs 71 (18):2531-2558
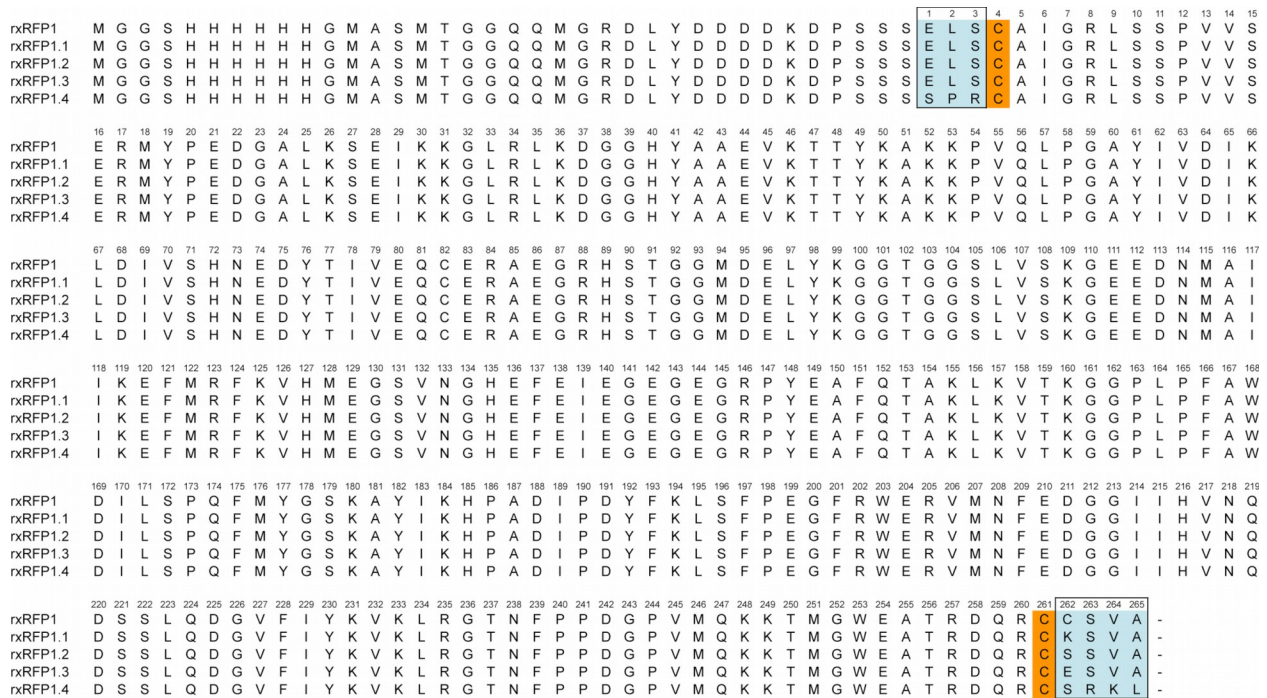
Figure 1. Sequence alignment of redox-sensitive red fluorescent protein mutants described in this work. Unnumbered N-terminal residues (including the His$_6$ Tag) are encoded in the plasmid backbone of pBAD/His B. Two key cysteine residues for reversible disulfide bond formation (residues 4 and 261) and amino acid residues varied among rxRFP mutants (residues 1-3 and 262-265) are highlighted in orange and cyan, respectively.
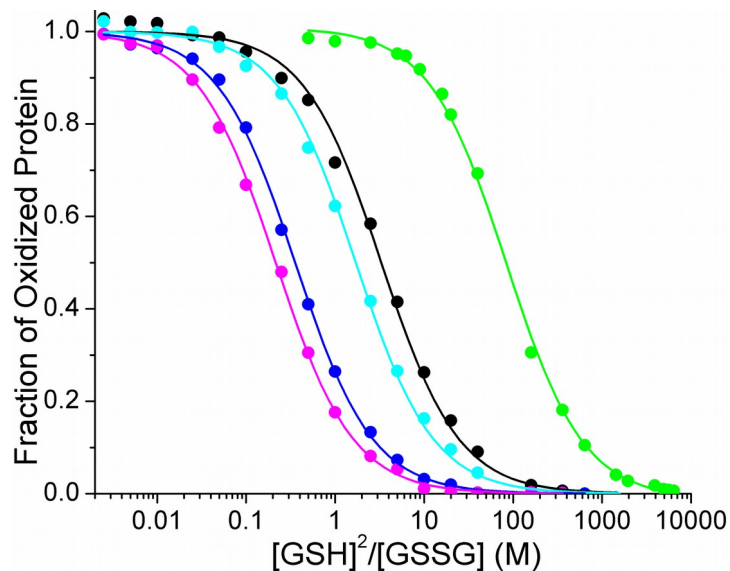
Figure 2. Redox titration of rxRFP mutants with reduced and oxidized glutathiones, showing different midpoint redox potentials for rxRFP1 (black), rxRFP1.1 (green), rxRFP1.2 (cyan), rxRFP1.3 (blue), and rxRFP1.4 (magenta). The fractions of oxidized proteins were determined based on fluorescence intensities of rxRFP mutants in equilibration with mixtures of reduced and oxidized glutathiones at pH 7.4.
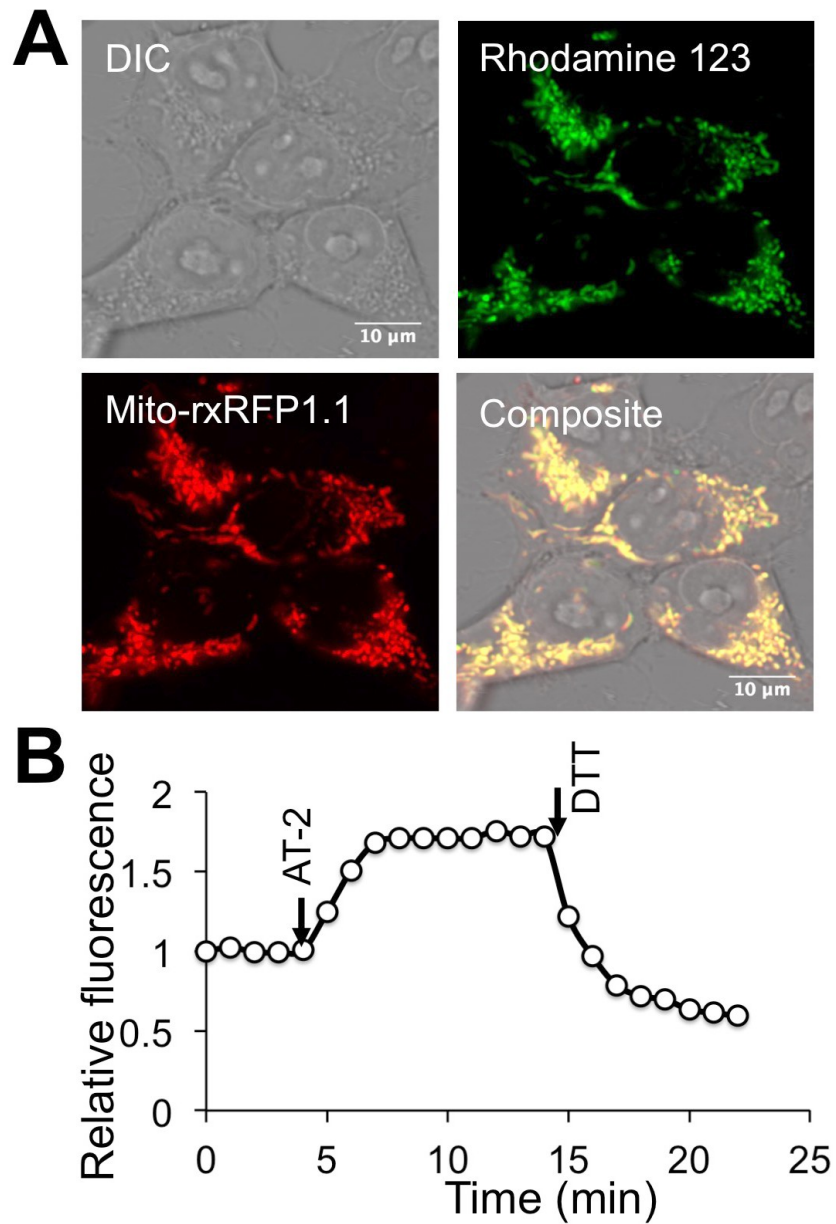
Figure 3. (**A**) Fluorescence imaging of HEK 293T cells, showing mitochondrial localization of rxRFP1.1. Rhodamine 123, a known mitochondrial probe, was used for comparison. (**B**) A representative trace of fluorescence intensities (normalized to the intensity value at 0 min) of a HEK 293T cell expressing mitochondrial rxRFP1.1, treated with AT-2 (1 mM) and DTT (10 mM) at 4 min and 14 min, respectively.
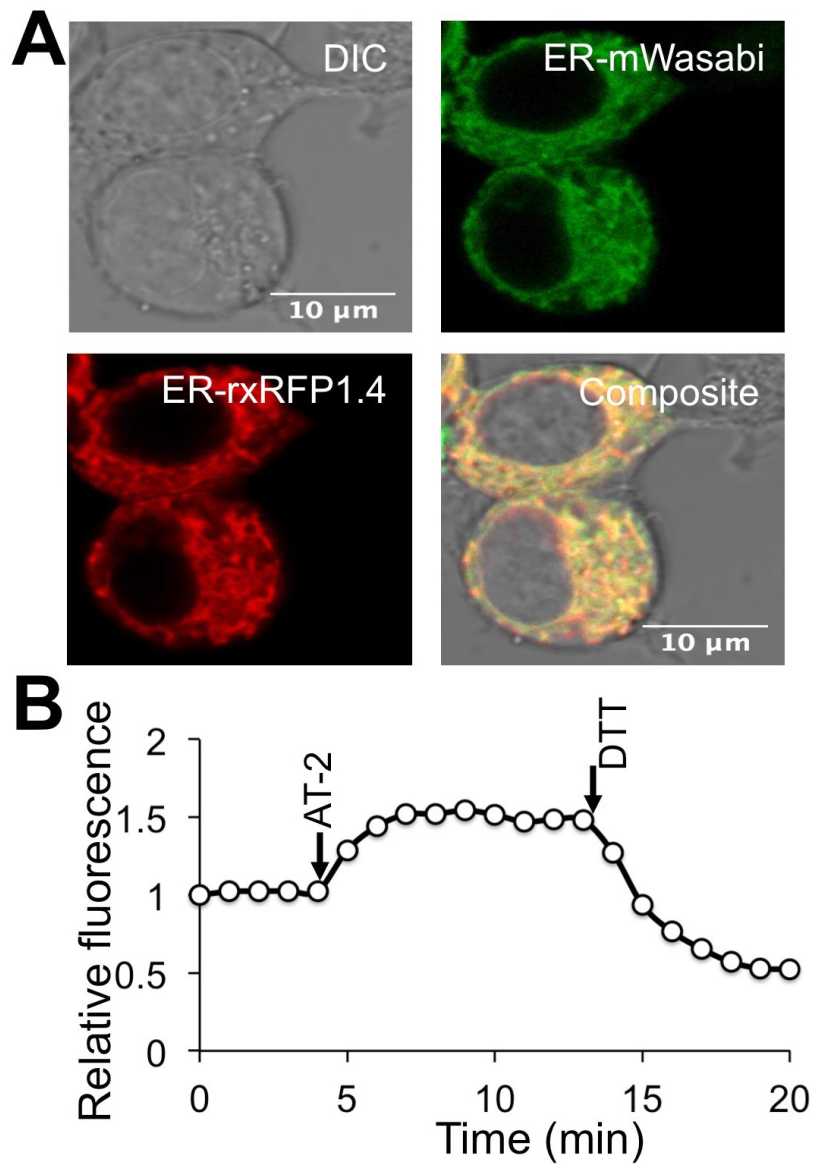
Figure 4. (**A**) Fluorescence imaging of HEK 293T cells, showing ER localization of rxRFP1.4. A previously validated green fluorescent ER-mWasabi probe was used for comparison. (**B**) A representative trace of fluorescence intensities (normalized to the intensity value at 0 min) of a HEK 293T cell expressing rxRFP1.4 in the ER, by addition of AT-2 (1 mM) and DTT (10 mM) in the culture medium at 4 min and 13 min, respectively.
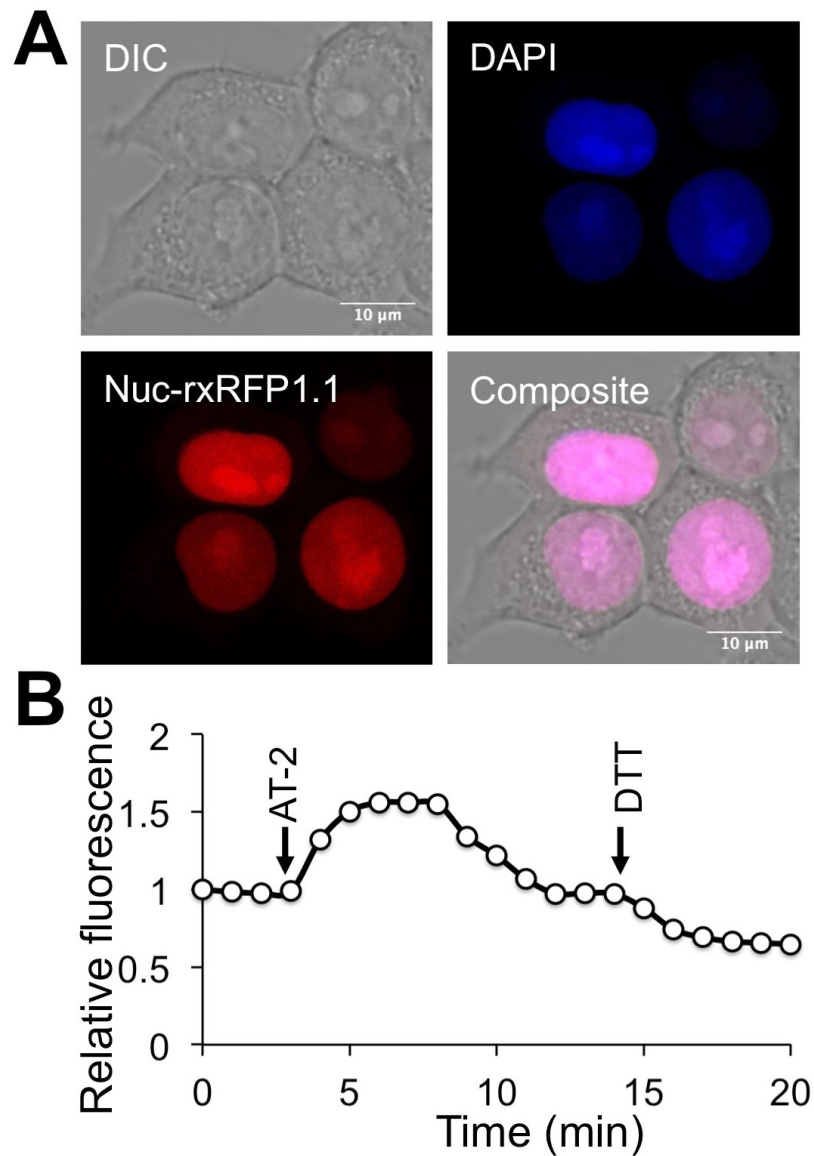
Figure 5. (**A**) Fluorescence imaging of HEK 293T cells, showing nuclear localization of rxRFP1.1. DAPI was also utilized to stain cell nuclei. (**B**) A representative trace of fluorescence intensities (normalized to the intensity value at 0 min) of a HEK 293T cell expressing nuclear rxRFP1.1, treated with AT-2 (1 mM) and DTT (10 mM) at 3 min and 14 min, respectively.
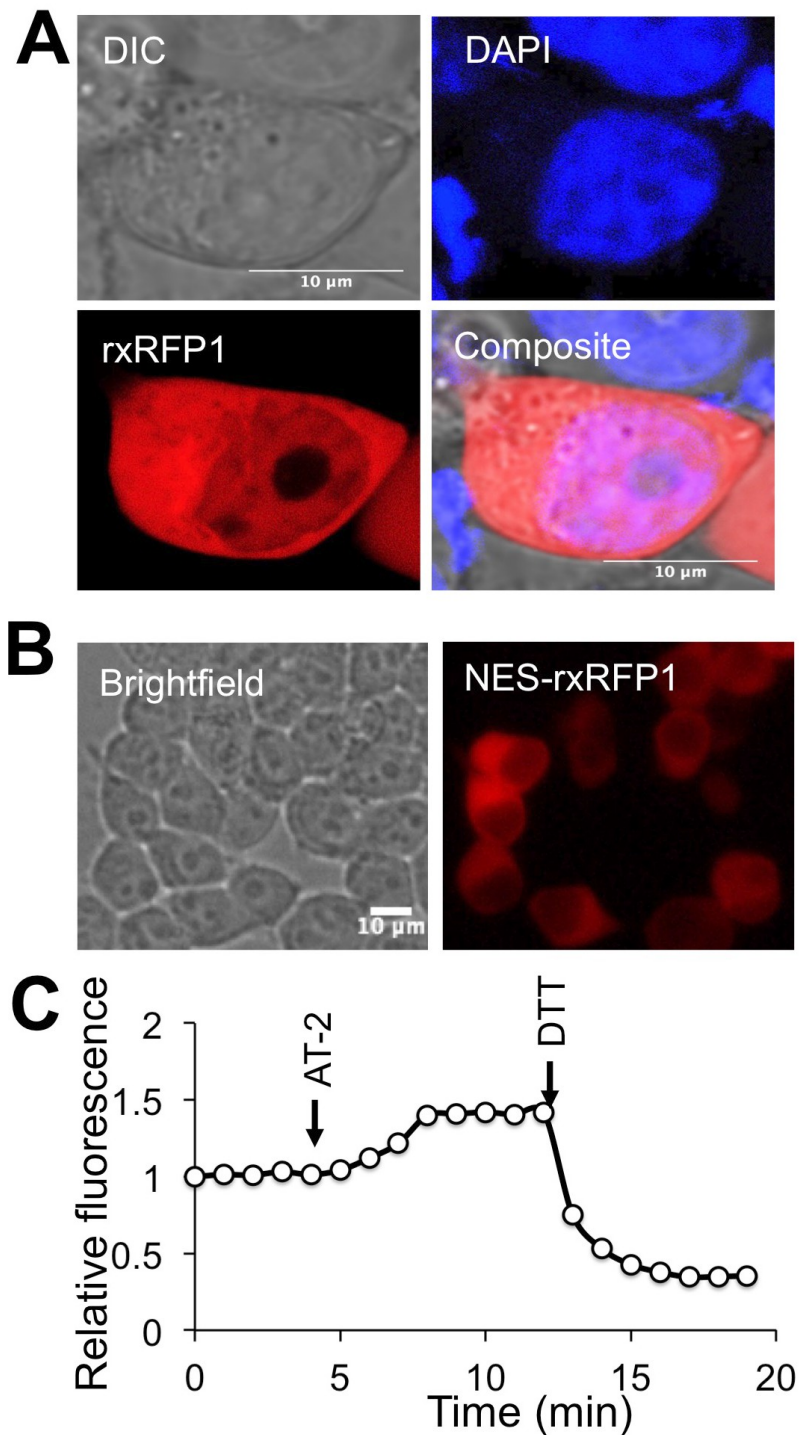
Figure 6. (**A**) Fluorescence imaging of HEK 293T cells expressing unlocalized rxRFP1. The cell nucleus was less fluorescence than the cytosol, and rxRFP1 seemed to be excluded from a condensed nuclear subdomain. (**B**) Fluorescence imaging of HEK 293T cells expressing rxRFP1 fused with nuclear export signal (NES). (**C**) A representative trace of fluorescence intensities (normalized to the intensity value at 0 min) of a HEK 293T cell expressing cytosolic rxRFP1, treated with AT-2 (1 mM) and DTT (10 mM) at 4 min and 12 min, respectively.
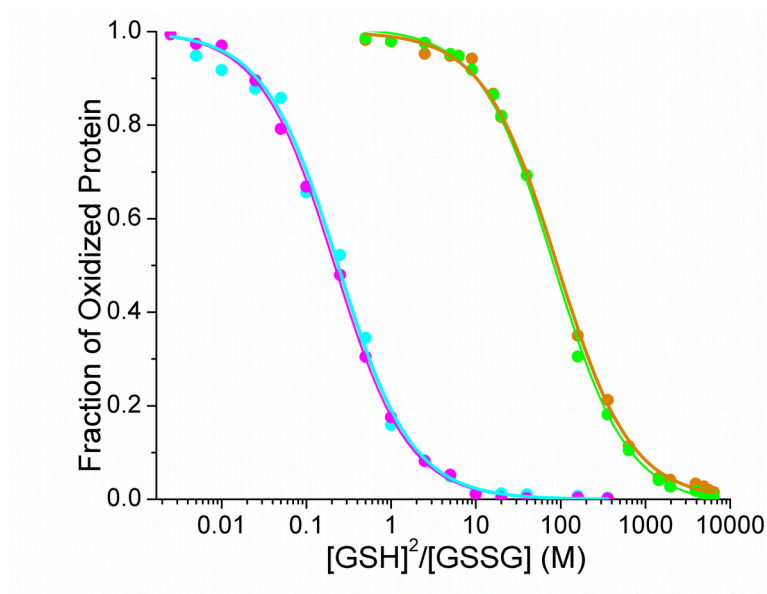
Figure 7. Redox titration of rxRFP1.1 with reduced and oxidized glutathiones at pH 7.4 (green) and pH 8 (dark orange), and rxRFP1.4 at pH 7.4 (magenta) and pH 7 (cyan), suggesting that the corresponding equilibrium was not shifted in these pH ranges.
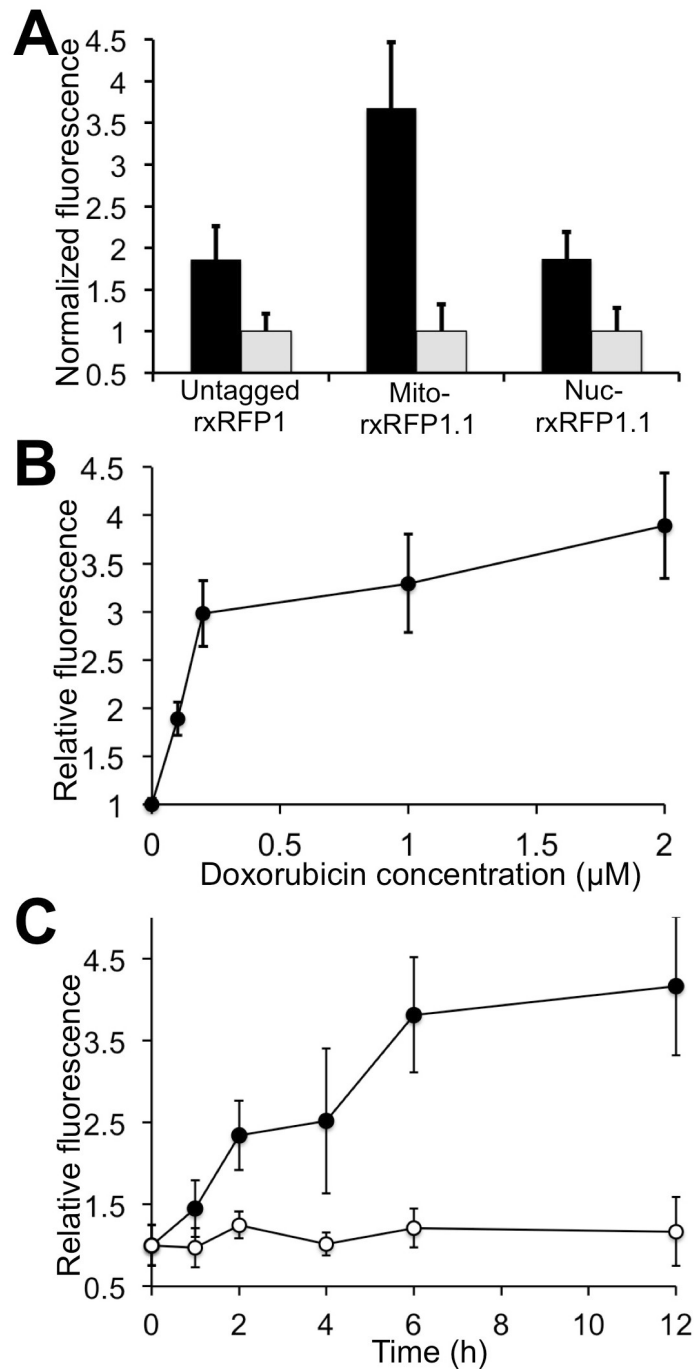
Figure 8. (**A**) Comparison of fluorescence intensities of cells expressed either untagged rxRFP1, or mitochondrial rxRFP1.1, or nuclear rxRFP1.1, and treated or untreated with doxorubicin (2 µM). Fluorescence intensities were normalized to the values of untreated cells in their corresponding groups. (**B**) Dose-dependent fluorescence increase of HEK 293T cells expressing mitochondrial rxRFP1.1. Fluorescence intensities were normalized to the values of untreated cells. (**C**) Time-dependent fluorescence increase of HEK 293T cells expressing mitochondrial rxRFP1.1, treated (filled circle) or untreated (open circle) with doxorubicin (2 µM). Fluorescence intensities were normalized to the values of untreated cells at 0 hs.

Table 1. Fluorescent properties of rxRFP and its mutants.

Protein		λ_{ab} (nm) with ε ($mM^{-1}cm^{-1}$) in parenthesis[a]	λ_{em} (nm) with Φ in parenthesis[a]	Brightness[b] ($mM^{-1}cm^{-1}$)	pK_a[c]	Dynamic range[d]	Midpoint potential (mV)[e]
rxRFP1.1	Oxidized	448 (30.1), 576 (33.0)	600 (0.18)	5.94	10.1	4.5×	− 324
	Reduced	448 (36.2), 576 (7.4)	600 (0.18)	1.33	10.2		
rxRFP1.2	Oxidized	448 (35.1), 576 (15.7)	600 (0.14)	2.20	9.2	3.8×	− 272
	Reduced	448 (37.5), 576 (4.1)	600 (0.14)	0.57	9.4		
rxRFP1.3	Oxidized	448 (34.9), 576 (14.4)	600 (0.13)	1.87	8.9	3.6×	− 251
	Reduced	448 (36.7), 576 (4.0)	600 (0.13)	0.52	8.8		
rxRFP1.4	Oxidized	448 (30.3), 576 (32.5)	600 (0.17)	5.53	8.9	4.1×	− 244
	Reduced	448 (36.1), 576 (8.0)	600 (0.17)	1.36	9.2		
rxRFP1	Oxidized	448 (34.3), 576 (26.0)	600 (0.14)	3.64	8.7	4.0×	− 281[f]
	Reduced	448 (36.7), 576 (6.5)	600 (0.14)	0.91	8.7		

[a] Measured at pH 7.4. [b] Defined as the product of ε and Φ. [c] Defined as the pH value at which 50% of the maximal fluorescence emission is maintained. [d] Defined as the ratio of emission intensities in the oxidized and reduced states at pH 7.4. [e] Derived from fluorescence measurements of proteins equilibrated with GSH and GSSG at pH 7.4. [f] Re-determined in this study for pH 7.4 and 37°C.

Table 2. Basal redox potentials of cellular compartments, estimated by using rxRFP mutants.

Cellular location	Probe used	Estimated basal redox potential (pH and temperature)
Mitochondria	Mitochondrial rxRFP1.1	− 365 mV (pH 7.98 and 37 °C)
Cell nucleus	Nuclear rxRFP1.1	− 326 mV (pH 7.4 and 37°C)
ER	ER-localized rxRFP1.4	− 209 mV (pH 7.0 and 37°C)
Cytosol	Cytosolic rxRFP1	− 277 mV (pH 7.4 and 37°C)